Journal of Power Sources 185 (2008) 1131–1140

Contents lists available at ScienceDirect

Journal of Power Sources

journal homepage: www.elsevier.com/locate/jpowsour

A transient two-phase mass transport model for liquid feed direct methanol fuel cells

W.W. Yang, T.S. Zhao*

Department of Mechanical Engineering, The Hong Kong University of Science and Technology, Clear Water Bay, Kowloon, Hong Kong SAR, China

ARTICLE INFO

Article history:
Received 30 April 2008
Received in revised form 11 July 2008
Accepted 15 July 2008
Available online 29 July 2008

Keywords:
Direct methanol fuel cell (DMFC)
Mass transport
Transient
Model

ABSTRACT

A transient two-phase mass transport model for liquid feed direct methanol fuel cells (DMFCs) is developed. With this model, various processes that affect the DMFC transient behaviors are numerically studied. The results show that the cell voltage exhibits an overshoot behavior in response to a sudden change in the current density. The magnitude of the overshoot depends on the magnitudes of the change in the cell current density and the initial current density. It is found that the dynamic change in the methanol permeation through the membrane to the cathode results in a strong cathode overpotential overshoot, which is believed to be the predominant factor that leads to the cell voltage overshoot. In contrast, the anode overpotential is relatively insensitive to the changes in the methanol concentration as well as CO surface coverage in the anode catalyst layer. Moreover, the effect of the double layer capacitance (DLC) on the cell dynamic behavior is studied and the results show that the DLC can smoothen the change in the cell voltage in response to a change in the cell current density. Furthermore, the dynamic response of mass transport to a change in the cell current density is found to be rather slow. In particular, it is shown that the slow response in the mass transport of methanol is one of the key factors that influence the cell dynamic operation.

1. Introduction

Because of its promising virtues for powering portable electronic devices, the direct methanol fuel cell (DMFC) has been extensively studied over the past decade, most of them focused on the fuel cell steady-state behaviors. As a matter of fact, the transient behaviors of the fuel cell associated with the change in operating conditions, such as system start-up, shut-down, sudden changes in the power level are also important and need to be investigated. A change in the cell operation conditions may result in the changes in the cell temperature and the reactant concentrations at the electrode surface, which eventually determine the overall transient response of the cell. A better understanding of the fuel cell dynamic characteristics under the transient operation conditions is thus essential, which enables the engineers to better design and control the fuel cell system. With this purpose, some experimental investigations of the DMFC dynamic operating characteristics have been reported. A widely used experimental method is to make a step change in the input parameter to the DMFC, such as the methanol feed concentration or the current density, and to study the response of the cell voltage. For instance, Sundmacher and co-workers studied the dynamic response of a DMFC with a step change in the methanol feed concentration [1,2]. Other researchers also investigated the dynamic behaviors of the DMFC by making a step change in the cell current density [3–5]. In response to the change in the cell current density, the cell voltage usually exhibited an overshoot behavior. Argyropoulos et al. [3,4] also studied the DMFC's response to the consecutive change in the current density in addition to the single step change in the current density. In addition, Kallo et al. [5] studied the cell voltage response of a gas feed DMFC to a step change in the cell current density. They also investigated the effects of the double layer capacitance (DLC), the formation/removal of CO poison on Pt catalyst at the anode, and the methanol crossover on the cell voltage response. Besides above-mentioned works, in-situ flow visualization studies [6] were also conducted to investigate the transient behaviors of two-phase flow in the flow field of the DMFC and its effect on the cell performance. It should be mentioned that electrochemical impedance spectroscopy (EIS) can also be used to study the dynamic cell behavior. Although EIS can cover a wide time range as well as monitoring of most processes occurring in the fuel cell, the quantitative interpretation and EIS modeling of the complete DMFC have not been achieved yet.

In addition to experimental efforts, mathematical modeling can be very useful in understanding both the steady-state and the

* Corresponding author. Tel.: +852 2358 8647; fax: +852 2358 1543.
E-mail addresses: yangww@ust.hk (W.W. Yang), metzhao@ust.hk (T.S. Zhao).

0378-7753/$ – see front matter © 2008 Elsevier B.V. All rights reserved.
doi:10.1016/j.jpowsour.2008.07.052

Nomenclature

A_{lg}	interfacial specific area between liquid and gas phase ($m^2\ m^{-3}$)
A_s	specific surface area of the active reaction sites ($m^2\ m^{-3}$)
C	molar concentration ($mol\ m^{-3}$)
C_{ACL}	double layer capacitance of anode catalyst layer ($C\ m^{-2}$)
C_{CCL}	double layer capacitance of anode catalyst layer ($C\ m^{-2}$)
D	diffusivity ($m^2\ s^{-1}$)
F	Faraday constant (96,478 $C\ mol^{-1}$)
$\mathbf{i}_+$	proton current vector in the catalyst layer ($A\ m^{-2}$)
$\mathbf{I}$	proton current vector in the membrane ($A\ m^{-2}$)
I_{cell}	cell current density ($A\ m^{-2}$)
I_{Para}	parasitic current resulting from methanol crossover ($A\ m^{-2}$)
j_0	exchange current density ($A\ m^{-2}$)
j_a	anode current density ($A\ m^{-3}$)
j_c	cathode current density ($A\ m^{-3}$)
k_{a1}	reaction rate constant for anode reaction step 1 ($mol\ m^{-2}\ s^{-1}$)
k_{a2}	reaction rate constant for anode reaction step 2 ($mol\ m^{-2}\ s^{-1}$)
k_c	condensation rate ($mol\ atm^{-1}\ s^{-1}\ m^{-3}$)
k_e	evaporation rate ($1\ atm^{-1}\ s^{-1}$)
k_H	Henry's law constant (Pa)
k_r	relative permeability
K	permeability of porous material (m^2)
$\dot{m}$	source term in mass conservation equation ($kg\ m^{-3}\ s^{-1}$)
M	molecular weight ($kg\ mol^{-1}$)
n_d	electro-osmotic drag coefficient
$\mathbf{N}$	vector flux of species ($mol\ m^{-2}\ s^{-1}$)
p_c	capillary pressure (Pa)
p_g	gas phase pressure (Pa)
p_l	liquid phase pressure (Pa)
R	gas constant ($J\ mol^{-1}\ K^{-1}$)
$\dot{R}$	source term in species conservation equation ($mol\ m^{-3}\ s^{-1}$)
$\tilde{R}$	interfacial species transfer rate ($mol\ m^{-3}\ s^{-1}$)
R_1	reaction rate of anode reaction step 1 ($mol\ m^{-2}\ s^{-1}$)
R_2	reaction rate of anode reaction step 2 ($mol\ m^{-2}\ s^{-1}$)
$R_{Contact}$	Ohmic contact resistance (Ωm^2)
s	liquid saturation
T	temperature (K)
$\vec{\mathbf{u}}_g$	velocity vector of gas phase ($m\ s^{-1}$)
$\vec{\mathbf{u}}_l$	velocity vector of liquid phase ($m\ s^{-1}$)
V_0	thermodynamic equilibrium voltage (V)
V_{cell}	cell voltage (V)
x	coordinate, m, or mole fraction in liquid solution ($mol\ mol^{-1}$)
y	coordinate, m, or mole fraction in gas mixture ($mol\ mol^{-1}$)

Greek letters

Γ	surface concentration of Pt ($mol\ m^{-2}$)
α	gas-void fraction ($1-s$)
α_a	anode transfer coefficient at anode
α_c	cathode transfer coefficient at cathode
δ	thickness of porous layer (m)
ε	porosity of porous medium
η	overpotential (V)
κ	ionic conductivity of membrane ($\Omega^{-1}\ m^{-1}$)
μ	viscosity ($kg\ m^{-1}\ s^{-1}$)
θ_c	contact angle (°)
θ_{CO}	surface coverage of CO species on the anode Pt catalysts
ρ	density ($kg\ m^{-3}$)
σ	interfacial tension ($N\ m^{-1}$)

Superscripts

eff	effective value
in	inlet condition
ref	reference value
sat	saturated value

Subscripts

A	anode
ACL	anode catalyst layer
ADL	anode diffusion layer
C	cathode
CCL	cathode catalyst layer
CDL	cathode diffusion layer
G	gas phase
L	liquid phase
Mem	membrane
M	methanol
MV	methanol vapor
W	water
WV	water vapor

dynamic behaviors of the DMFC. Most of the existing DMFC models are restricted to steady-state condition [7–20], and the transient models for DMFCs are scarce. Sundmacher et al. [21] developed a model to study the voltage response to a change in the methanol feed concentration. The results revealed that the voltage underwent an overshoot in response to a step change in the methanol feed concentration. Schultz et al. [22] also studied the voltage response to a step change in the methanol feed concentration. Their one-dimensional, multi-component mass transport model was developed based on the Maxwell–Stefan equation. The model-based analysis revealed that the cell voltage overshoot was resulted from the different time responses of the anode and cathode overpotentials to the change in the methanol concentration. In addition to the studies with a step change in the methanol feed concentration, other researchers also developed mathematical models to study the dynamic voltage response of the DMFC to a change in the cell current density. For instance, Krewer and Sundmacher [23] numerically revealed that the methanol crossover is the dominating factor that causes the cathode overpotential overshoot and then the cell voltage overshoot. This result is consistent with the experimental study by Kallo et al. [5]. More recently, Krewer et al. [24] presented another model to investigate the voltage response to a change in the cell current density, and showed that the anode reaction mechanism was the main physicochemical phenomena that cause the anode overpotential overshoot, hence the cell voltage overshoot. However, this result was somewhat contradictory to their earlier study [23]. It is also worth mentioning that a few transient models for studying the start-up process of passive DMFCs have also been reported [25,26].

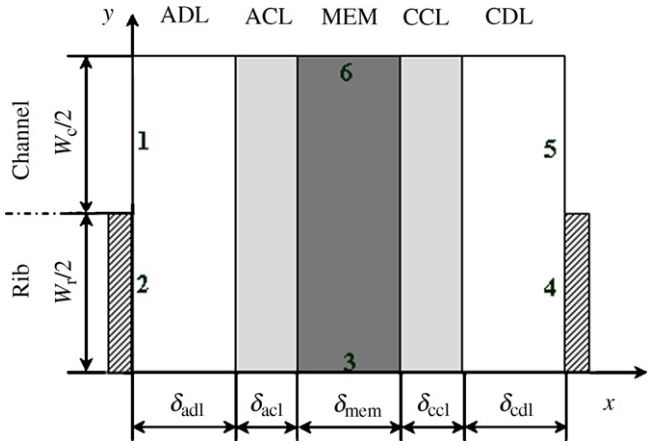

Fig. 1. Schematic of the model domain. Roman numerals refer to the boundaries of the modeling geometries.

Our literature review indicates that most previous transient transport models for DMFCs [23,24,27] assume that the transport of methanol through the anode diffusion layer, catalyst layer and the membrane is fast enough and can be treated as a quasi-steady process. This assumption is questionable as the mass transport of species is usually much slower than the charge processes and electrochemical processes at the electrode [27]. Also, we found that the interpretations to the voltage overshoot behavior by different models are contradictory. Motivated by addressing these problems, in this work we developed a transient, two-dimensional, two-phase mass transport model for DMFCs, in which the assumption of quasi-steady mass transport is eliminated. With this model, various processes that affect the DMFC transient operating behaviors are numerically studied.

2. Formulation

Consider a two-dimensional physical domain, as sketched in Fig. 1, which represents the typical geometry of a membrane electrode assembly (MEA) that consists of anode diffusion layer (ADL), an anode catalyst layer (ACL), a membrane (MEM), a cathode catalyst layer (CCL), and a cathode diffusion layer (CDL). The MEA is sandwiched between two parallel flow field plates. Since both channel width and rib width in the parallel flow-field are symmetrical with respect to their middle points, only a half-rib width and a half-channel width need to be considered to save the computing cost.

2.1. Anode porous region

In the anode porous region (the anode diffusion and catalyst layers), we are interested in four major variables, including liquid methanol concentration ($C_{M,l}$), methanol vapor concentration ($C_{M,g}$), liquid saturation and liquid pressure (p_l). The general governing equations corresponding to each of these variables are given by

$$C_{M,l}: \frac{\partial}{\partial t}(\varepsilon s_{l,a} C_{M,l}) = -\nabla \cdot \mathbf{N}_{M,l} + \dot{R}_{M,l} \tag{1}$$

$$C_{M,g} = \frac{\partial}{\partial t}[\varepsilon(1-s_{l,a})C_{M,g}] = -\nabla \cdot \mathbf{N}_{M,g} + \dot{R}_{M,g} \tag{2}$$

$$s_{l,a}: \frac{\partial}{\partial t}[\rho_g \varepsilon(1-s_{l,a})] = \nabla \cdot \left[\rho_g K \frac{k_{rg}}{\mu_g}\left(\frac{dp_c}{ds}\nabla \cdot s_{l,a} + \nabla \cdot p_l\right)\right] + \dot{m}_{g,a} \tag{3}$$

$$p_{l,a}: \frac{\partial}{\partial t}(\rho_l \varepsilon s_{l,a}) = \nabla \cdot \left(\rho_l K \frac{k_{rl}}{\mu_l} \cdot \nabla \cdot p_{l,a}\right) + \dot{m}_{l,a} \tag{4}$$

where $\mathbf{N}_{M,l}$ and $\mathbf{N}_{M,g}$ are both vectors, representing the transport flux of methanol and methanol vapor in the anode electrode, respectively. Taking into account the main transport mechanism of methanol, namely, the molecular diffusion, macroscopic convection and electro-osmotic drag, the overall flux of methanol and methanol vapor can be, respectively, calculated from

$$\mathbf{N}_{M,l} = \begin{cases} C_{M,l}\vec{\mathbf{u}}_l - D^{eff}_{M,l}\nabla \cdot C_{M,l} & \text{ADL} \\ C_{M,l}\vec{\mathbf{u}}_l - D^{eff}_{M,l}\nabla \cdot C_{M,l} + n_{d,w}x_M\dfrac{\mathbf{i}_+}{F} & \text{ACL} \end{cases} \tag{5}$$

and

$$\mathbf{N}_{M,g} = C_{M,g}\vec{\mathbf{u}}_g - D^{eff}_{M,g}\nabla \cdot C_{M,g} \tag{6}$$

To account for the effect of methanol evaporation and condensation, the interfacial transfer rate of methanol between the liquid and gas phase is given by:

$$\tilde{R}_M = A_{lg}h_{lg}s(1-s)\frac{(p^{sat}_{MV} - p_{MV})}{RT} \tag{7}$$

where p^{sat}_{MV} denotes the saturation pressure of methanol vapor. Note that the interfacial transfer of methanol between the phases is finally embodied in the general source terms on the right-hand sides of Eqs. (1)–(4).

2.2. Cathode porous region

The two-phase mass transport behaviors in the cathode porous region (the cathode diffusion and catalyst layer) are related to four major variables, i.e., oxygen concentration ($C_{O_2,g}$), water vapor concentration ($C_{WV,g}$), liquid saturation (s_l) and gas pressure (p_g). The governing equations of conservation corresponding to the four variables are, respectively, given by:

$$C_{O_2,g}: \frac{\partial}{\partial t}[\varepsilon(1-s_{l,c})C_{O_2,g}] = -\nabla \cdot \mathbf{N}_{O_2,g} + \dot{R}_{O_2,g} \tag{8}$$

$$C_{WV,g}: \frac{\partial}{\partial t}[\varepsilon(1-s_{l,c})C_{WV,g}] = -\nabla \cdot \mathbf{N}_{WV,g} + \dot{R}_{O_2,g} \tag{9}$$

$$s_{l,c}: \frac{\partial}{\partial t}(\rho_l \varepsilon s_{l,a}) = \nabla \cdot \left[\rho_l K \frac{k_{rl}}{\mu_l} \cdot \left(-\frac{dp_c}{ds}\nabla s_{l,c} + \nabla \cdot p_{g,c}\right)\right] + \dot{m}_{l,c} \tag{10}$$

$$p_{g,c}: \frac{\partial}{\partial t}[\rho_g \varepsilon(1-s_{l,c})] = \nabla \cdot \left(\rho_g K \frac{k_{rg}}{\mu_g} \cdot \nabla \cdot p_{g,c}\right) + \dot{m}_{g,c} \tag{11}$$

where $\mathbf{N}_{O_2,g}$ and $\mathbf{N}_{WV,g}$ are both vectors, denoting the transport flux of gas oxygen and water vapor in the cathode porous region, which can be obtained from:

$$\mathbf{N}_{i,g} = C_{i,g}\vec{\mathbf{u}}_g - D^{eff}_{i,g}\nabla \cdot C_{i,g} \quad i: O_2, WV \tag{12}$$

To consider the effect of water evaporation and condensation, the interfacial transfer rate of water between the liquid and gas phase is given by [28,29]:

$$\tilde{R}_w = \begin{cases} k_e\dfrac{\varepsilon s \rho_l}{M_{H_2O}}(y_{WV}p_g - p^{sat}_{WV}) & y_{WV}p_g < p^{sat}_{WV} \\ k_c\dfrac{\varepsilon(1-s)y_{WV}}{RT}(y_{WV}p_g - p^{sat}_{WV}) & y_{WV}p_g > p^{sat}_{WV} \end{cases} \tag{13}$$

where p^{sat}_{WV} and y_{WV} denote the saturation pressure of water vapor and mole fraction of water vapor in the cathode gas phase, respectively. Note that the interfacial transfer of water between the phases is embodied in the source terms on the right-hand sides of Eqs. (8)–(11).

Table 1
Constitutive relations

Parameters	Expressions
Capillary pressure	$p_c = p_g - p_l = \sigma \cos\theta_c (\varepsilon/K)^{0.5} J(s)$ $J(s) = \begin{cases} 1.417(1-s) - 2.120(1-s)^2 + 1.263(1-s)^3 & 0 < \theta_c \le 90^\circ \\ 1.417s - 2.120s^2 + 1.263s^3 & 90^\circ < \theta_c < 180^\circ \end{cases}$
Relative permeabilities	$k_{rl} = s^3$ Liquid $k_{rg} = (1-s)^3$ Gas
Effective diffusion coefficients of species [18]	$D_{i,g}^{eff} = D_{i,g}\varepsilon^{1.5}(1-s)^{1.5}$ i : O_2, WV, MV
	$D_M^{eff} = \begin{cases} D_{M,l}\varepsilon^{1.5}s^{1.5} & \text{ADL} \\ \dfrac{(\varepsilon+\varepsilon_N)}{[\varepsilon/(D_{M,l}\varepsilon^{1.5}s^{1.5}) + \varepsilon_N/(D_{M,N}\varepsilon_N{}^{1.5})]} & \text{ACL} \\ D_{M,N}\varepsilon^{1.5} & \text{MEM} \end{cases}$
General generation rate of mass in liquid phase	$\dot{m}_{l,a} = \begin{cases} -M_{H_2O}\tilde{R}_W - M_M\tilde{R}_M & \text{ADL} \\ -(M_{H_2O}+M_M)\dfrac{j_a}{6F} - M_{H_2O}\tilde{R}_W - M_M\tilde{R}_M & \text{ACL} \end{cases}$
	$\dot{m}_{l,c} = \begin{cases} -M_{H_2O}\tilde{R}_W & \text{CDL} \\ M_{H_2O}\left(\dfrac{j_c}{2F} - \dfrac{I_p}{6F\delta_{ccl}}\right) - M_{H_2O}\tilde{R}_W & \text{CCL} \end{cases}$
General generation rate of mass in gas phase	$\dot{m}_{g,a} = \begin{cases} M_{H_2O}\tilde{R}_W - M_M\tilde{R}_M & \text{ADL} \\ M_{CO_2}\dfrac{j_a}{6F} - M_{H_2O}\tilde{R}_W - M_M\tilde{R}_M & \text{ACL} \end{cases}$
	$\dot{m}_{g,c} = \begin{cases} M_{H_2O}\tilde{R}_W & \text{CDL} \\ -M_{O_2}\dfrac{j_c}{4F} + M_{CO_2}\dfrac{I_p}{6F\delta_{ccl}} - M_{H_2O}\tilde{R}_W & \text{CCL} \end{cases}$
Mole generation rate of species	$\dot{R}_{O_2} = \begin{cases} 0 \\ -\dfrac{j_c}{4F} \end{cases}$, $\dot{R}_{WV,c} = \begin{cases} \tilde{R}_W & \text{CDL} \\ \tilde{R}_W & \text{CCL} \end{cases}$
	$\dot{R}_{M,l} = \begin{cases} -\tilde{R}_M \\ -\dfrac{j_a}{6F} - \tilde{R}_M \end{cases}$, $\dot{R}_{MV,a} = \begin{cases} \tilde{R}_M \\ \tilde{R}_M \end{cases}$, $\dot{R}_{WV,a} = \begin{cases} \tilde{R}_W & \text{ADL} \\ \tilde{R}_W & \text{ACL} \end{cases}$

2.3. Membrane

Unlike in the anode and cathode electrode, in the membrane, only transport of liquid phases (dissolved methanol and liquid water) needs to be considered as the membrane is usually regarded as a gas insulator. The mass conservation of dissolved methanol is described by:

$$\frac{\partial}{\partial t}(\varepsilon_{mem} C_{MeOH}) = -\nabla \cdot \mathbf{N}_M \tag{14}$$

with $\mathbf{N}_M$ denoting the vector flux of methanol in the membrane. Generally, transport of methanol through the membrane depends on molecular diffusion, electro-osmotic drag and convection, and the last one is usually negligible. Accordingly, the flux of methanol in the membrane is given by

$$\mathbf{N}_M = -D_{M,N}^{eff} \cdot \nabla C_{MeOH} + n_{d,M}\frac{\mathbf{I}}{F} \tag{15}$$

With respect to the water transport through the membrane, the flux due to the molecular diffusion can be ignored if the membrane is in equilibrium with liquid water on the both sides. Hence, the flux of water across the membrane ($\mathbf{N}_W$) is given by:

$$\mathbf{N}_W = n_{d,H_2O}\frac{\mathbf{I}}{F} - \frac{\rho_l}{M_{H_2O}}\frac{K}{\mu_l}\frac{\Delta p_{l,c-a}}{\delta_{mem}} \tag{16}$$

Up to this point, we have presented all the governing equations that describe the dynamic two-phase mass transport processes in a DMFC. To make the above governing equations closed, some constitutive correlations and definitions are needed. These include capillary pressure, relative permeability for both gas and liquid phase, effective diffusion coefficients for each species and the source terms. All these correlations and associated nomenclatures are clearly listed in Table 1.

2.4. Boundary conditions

As indicated in Fig. 1, the computational domain is enclosed by six boundaries. The boundary conditions at each boundary are described below.

Boundary 1: This boundary represents the inlet of reactant supply at the anode, at which the concentration of liquid methanol, the concentrations of methanol vapor, liquid-phase pressure and liquid saturation are all specified to be inlet conditions:

$$C_{M,l} = C_M^{in}, C_{MV} = C_{MV}^{in}, \quad s = 1, p_l = p_l^{in} \tag{17}$$

Boundary 2: This boundary is the interface between anode diffusion layer and the anode rib collector, which is an impermeable wall. Accordingly, all the fluxes in the x direction are zero at this boundary:

$$\frac{\partial C_M}{\partial x} = 0, \ \frac{\partial C_{MV}}{\partial x} = 0, \ \frac{\partial s}{\partial x} = 0, \ \frac{\partial p_l}{\partial x} = 0 \tag{18}$$

Boundaries 3 and 6: These two boundaries are symmetrical, respectively, with respect to the middle point of rib width and the middle point of channel width. Hence, the gradients of all the variables in y direction are set to zero:

$$\frac{\partial \phi}{\partial y} = 0 \quad \phi : C_{M,l}, \ C_{MV}, \ s, \ p_l, \ C_{O_2}, \ C_{WV}, \ p_g \tag{19}$$

Boundary 4: Similar to Boundary 2, Boundary 4 represents the interface between cathode diffusion layer and the cathode rib collector, at which all the fluxes in the x direction are zero:

$$\frac{\partial C_{O_2}}{\partial x} = 0, \ \frac{\partial C_{WV}}{\partial x} = 0, \ \frac{\partial s}{\partial x} = 0, \ \frac{\partial p_g}{\partial x} = 0 \tag{20}$$

Boundary 5: This boundary represents the inlet of oxygen supply and outlet of water removal at the cathode, at which the following boundary conditions are specified:

$$C_{O_2} = C_{O_2}^{in}, C_{WV} = C_{WV}^{in}, s = 0, p_g = p_g^{in} \tag{21}$$

The conditions at the interfaces between those functional layers in the 'sandwiched' cell are given based on the principle that the continuity and mass/species flux balance are required at each interface to satisfy the general mass and species conservation of the entire cell. The more details can be found elsewhere [18].

2.5. Electrochemical kinetics

On the DMFC anode, a simplified two-step reaction mechanism is used to describe the electrochemical oxidation of methanol at the platinum-ruthenium catalysts in the anode [1]. In the first irreversible step, methanol is adsorbed electrochemically to the platinum catalyst, forming strongly adsorbed carbon monoxide, four protons and four electrons.

$$CH_3OH + Pt \rightarrow CH_3OH_{ads} \xrightarrow{R_1} CO_{ads} + 4H^+ + 4e^- \quad (1)$$

The second step is a combination of two consecutive reactions: (a) water adsorbs electrochemically to the ruthenium catalyst in a reversible reaction to form OH_{ads}, a proton and an electron, (b) the formed OH_{ads} the reacts irreversibly with CO_{ads} to form carbon dioxide, proton and electron. In these two consecutive reactions, the reaction (b) is assumed to be the rate-determining step, while the reaction (a) is assumed always in quasi-equilibrium. Simply, the overall reaction of the second step is described by:

$$CO_{ads} + H_2O \xrightarrow{Ru, R_2} CO_2 + 2H^+ + 2e^- + Pt \quad (2)$$

Since both the reactions steps are irreversible electrochemical reactions, their rate expressions are formulated in the form of Tafel kinetics. To consider the effect of the adsorption and desorption of species to the platinum catalyst surface, the rate expressions also contain a term to account for the influence of the surface coverage of the platinum catalyst with adsorbed CO. The details are as follows.

$$R_1 = k_{a1} \frac{C_{MeOH}}{C^{ref}_{MeOH}} (1 - \theta_{CO}) \exp\left(\frac{\alpha_{a1} F}{RT} \eta_a\right) \quad (22)$$

$$R_2 = k_{a2} \theta_{CO} \exp\left(\frac{\alpha_{a2} F}{RT} \eta_a\right) \quad (23)$$

where θ_{CO} represents the surface coverage of platinum catalyst with adsorbed CO species. Note that the overpotential η_a in Eqs. (22) and (23) is the absolute difference between the real potential and the thermodynamic-equilibrium potential of MOR which are referenced to a standard hydrogen electrode (SHE).

The overall balance of θ_{CO} is then given by:

$$\Gamma \frac{d\theta_{CO}}{dt} = R_1 - R_2 \quad (24)$$

Taking into account the current generated in both reaction steps, the kinetics of the anodic reductive reaction can be expressed by

$$j_a = (4FA_s) k_{a1} \frac{C_{MeOH}}{C^{ref}_{MeOH}} (1 - \theta_{CO}) \exp\left(\frac{\alpha_{a1} F}{RT} \eta_a\right) + (2FA_s) k_{a2} \theta_{CO} \exp\left(\frac{\alpha_{a2} F}{RT} \eta_a\right) \quad (25)$$

with A_s denoting the specific surface area of active reaction sites.

On the DMFC cathode, the kinetics of oxygen reduction reaction (ORR) can be described by first-order Tafel expression

$$j_c = A_s j^{ref}_{0,O_2} \left(\frac{C_{O_2}/k_{H,O_2}}{C^{ref}_{O_2}}\right) \exp\left(\frac{\alpha_c F}{RT} \eta_c\right) \quad (26)$$

where C_{O_2} represents oxygen concentration in the gas pores. The term k_{H,O_2} denotes the Henry factor to capture the effect of dissolving process. The overpotential η_c in Eq. (26) represents the absolute difference between the real potential and the thermodynamic-equilibrium potential of ORR which are also referenced to a SHE.

In addition to the ORR, a second undesired reaction also takes place in the CCL, i.e., methanol crossover to the cathode is electro-oxidized. This parasitic reaction is usually very fast so that the methanol crossover is immediately and entirely consumed in the cathode. Notice that this parasitic reaction ultimately results in the cathode mixed overpotential.

2.6. Cell current density and cell voltage

The equivalent circuit for a DMFC can usually be simplified to a series connection of the membrane resistance and two capacitor/resistance parallel circuits corresponding to the double layer capacitance and the charge transfer resistance for the anode and cathode, respectively. Under dynamic operations, the charging/discharging process of the DLC may occur, accompanying the dynamic variation in the electrode potential. If true, part of the current will be used to charge the DLC or released from the DLC. Consequently, the dynamic cell current density satisfies

$$C_{ACL} \frac{d\eta_a}{dt} = I_{cell} - \frac{\iint_{ACL} j_a dx dy}{(W_c + W_r)/2} \quad (27)$$

where C_{ACL} represents the DLC of the anode electrode. Note the first term on the left-hand side of the Eq. (27) represents the current required for charging/discharging of the DLC, which will vanish at the steady-state operation.

As mentioned earlier, methanol may permeate through the membrane to the cathode. Usually, the 'parasitic' current density is used to represent the rate of methanol crossover because this part of current cannot be used to do work. On the DMFC cathode, it is assumed that both the cell current and the 'parasitic' current are entirely consumed by the ORR. With taking into account the impact of the double layer capacitance in the cathode electrode, the overall dynamic current balance is thus given by:

$$C_{CCL} \frac{d\eta_c}{dt} = I_{cell} + I_{para} - \frac{\iint_{CCL} j_c dx\, dy}{(W_c + W_r)/2} \quad (28)$$

with I_{para} denoting the 'parasitic' current density, which can be determined by:

$$I_{para} = \frac{6F \int_0^{(W_c+W_r)/2} N_M|_{MEM/CCL} dx}{(W_c + W_r)/2} \quad (29)$$

In summary, for a given dynamic cell current density, the dynamic anode overpotential can be determined from Eq. (27), while the dynamic cathode overpotential can be obtained from Eq. (28). Finally, the dynamic cell voltage can be obtained from

$$V_{Cell} = V_0 - \eta_a - \eta_c - I_{Cell}\left(R_{Contact} + \frac{\delta_{mem}}{\kappa}\right) \quad (30)$$

where V_0, $R_{Contact}$ and κ denote the thermodynamic equilibrium voltage of a DMFC, the contact resistance and the proton conductivity of the membrane, respectively.

3. Results and discussion

The above described governing equations for the cell geometric dimensions and operating parameters listed in Table 2 subjected to the boundary conditions, along with the constitutive relations shown in Table 1 and the physicochemical properties listed in Table 3, are solved numerically using a self-written code, which was developed based on the SIMPLE algorithm with the finite-volume-method. Note that the present transient DMFC model is extended

Table 2
Cell geometric dimensions and operating parameters

Parameters	Symbols	Value	Unit
Anode diffusion layer thickness	δ_{adl}	3.0×10^{-4}	m
Anode catalyst layer thickness	δ_{acl}	0.2×10^{-4}	m
Membrane thickness	δ_{mem}	1.8×10^{-4}	m
Cathode diffusion layer thickness	δ_{cdl}	2.6×10^{-4}	m
Cathode catalyst layer thickness	δ_{ccl}	0.2×10^{-4}	m
Channel width	w_c	1.0×10^{-3}	m
Rib width	w_r	1.0×10^{-3}	m
Operation temperature	T	333.15	K
Anode inlet pressure	p_l^{in}	1.013×10^5	Pa
Cathode inlet pressure	p_g^{in}	1.013×10^5	Pa
Inlet methanol concentration at anode	C_M^{in}	500	mol m^{-3}
Inlet methanol vapor concentration	C_{MV}^{in}	C_{MV}^{sat}	mol m^{-3}
Inlet oxygen concentration at cathode	$C_{O_2}^{in}$	7.35	mol m^{-3}
Inlet water vapor concentration at anode	C_{WV}^{in}	C_{WV}^{sat}	mol m^{-3}
Inlet water vapor concentration at cathode	C_{WV}^{in}	0	mol m^{-3}
Inlet liquid saturation at anode	s^{in}	1	–
Inlet liquid saturation at cathode	s^{in}	0	–

from our steady-state DMFC model developed earlier [30,31], which have proved to be competent in predicting the steady-state mass transport behaviors in a liquid DMFC.

3.1. Dynamic behavior of the cell voltage

Fig. 2 shows the time-dependent behavior of the cell voltage in response to the step changes in current density from 100, 75 or 50 mA cm^{-2} to a constant value of 10 mA cm^{-2}. As seen from this figure, in response to each change in current density the cell voltage sharply rises to a temporarily higher value and then gradually lowers to a stable value. Such a behavior has been termed as the voltage overshoot resulting from a dynamic load change. Also, it is found that a larger step change in the cell current leads to stronger overshoot behavior in the cell voltage. With respect to the time characteristic of the dynamic voltage response, it takes over 30 s for the cell voltage to reach a new steady-state for all the cases studied, closer to that observed experimentally [23], but six times longer than that predicted by other models [23,24,27], in which the mass transport processes were assumed to be sufficiently fast such that the processes can be treated as a quasi-steady-state. Apparently, this assumption of fast mass transport can result in a significant error in predicting the cell dynamic behavior. The time characteristic of the mass transport processes will be discussed later. Fig. 3 also presents the voltage overshoot behaviors in response to other four step changes in current density from 60 to 10 mA cm^{-2}, from 70 to 20 mA cm^{-2}, from 80 to 30 mA cm^{-2}, and from 90 to

Table 3
Physicochemical properties

Parameters	Symbols	Value	Unit	Ref.
Porosity, permeability				
ADL	ε_{adl}, K_{adl}	0.7, 2.0×10^{-12}	–, m^2	[33]
ACL	ε_{acl}, K_{acl}	0.3, 1.0×10^{-14}	–, m^2	
MEM	ε_{mem}, K_{mem}	0.3, 2.0×10^{-18}	–, m^2	
CCL	ε_{ccl}, K_{ccl}	0.3, 1.0×10^{-14}	–, m^2	
CDL	ε_{cdl}, K_{cdl}	0.7, 2.0×10^{-12}	–, m^2	[33]
Nafion volume fraction in ACL	$\varepsilon_{N,acl}$	0.4	–	
MeOH in water	$D_{M,l}$	$10^{-5.4163-999.778/T}$	m^2 s^{-1}	[14]
MeOH in Nafion	$D_{M,N}$	$4.9\times10^{-10}\,e^{[2436(1/333-1/T)]}$	m^2 s^{-1}	[34]
Methanol vapor	$D_{M,g}$	$-6.954\times10^{-6}+4.5986\times10^{-8}T+9.4979\times10^{-11}T^2$	m^2 s^{-1}	[14]
Diffusivities				
O_2 in gas	$D_{O_2,g}$	$1.775\times10^{-5}\left(\frac{T}{273.15}\right)^{1.823}$	m^2 s^{-1}	[14]
Water vapor in gas	$D_{wv,g}$	$2.56\times10^{-5}\left(\frac{T}{307.15}\right)^{2.334}$	m^2 s^{-1}	[14]
Viscosity of gas phase	μ_g	2.03×10^{-5}	kg m^{-1} s^{-1}	[36]
Viscosity of liquid phase	μ_l	4.05×10^{-4}	kg m^{-1}s^{-1}	[35]
Electro-osmotic drag coefficients of water and methanol	n_{d,H_2O}	2.5	–	[37]
	$d_{d,M}$	$n_{d,H_2O}x_M$	–	[37]
Reaction rate constant for anode reaction step 1	k_{a1}	1.6×10^{-3}	mol m^{-2} s^{-1}	[1]
Reaction rate constant for anode reaction step 1	k_{a2}	8.0×10^{-5}	mol m^{-2} s^{-1}	[1]
Condensation rate constant for water	k_c	5.0×10^{-5}	mol atm^{-1} s^{-1} cm^{-3}	[13]
Evaporation rate constant for water	k_e	5.0×10^{-3}	atm^{-1} s^{-1}	[13]
Henry law constant for oxygen	k_{H,O_2}	$e^{(-666/T+14.1)}/R/T$	–	[38]
Henry law constant for methanol	$k_{H,M}$	$0.096e^{0.04511(T-273)}$	atm	[14]
Double layer capacitance of ACL	C_{ACL}	1827	C m^{-2}	[23]
Double layer capacitance of CCL	C_{CCL}	907	C m^{-2}	[23]
Surface concentration of Pt catalyst	Γ_{Pt}	0.11	mol m^{-2}	[1]
Interfacial transfer rate constant for methanol	h_{1g}	0.001	m^2 s^{-1}	[16]
Specific interfacial area between liquid and gas	A_{1g}	10^5	m^{-1}	[16]
Specific surface area of anode catalyst	A_s	5000	m^{-1}	
Proton conductivity in membrane	κ	$7.3e^{[1268(1/298-1/T)]}$	Ω^{-1} m^{-1}	[34]
The saturation pressure of water vapor	$\log_{10}P_{WV}^{sat}$	$-2.1794+0.02953(T-273)-9.1837\times10^{-5}(T-273)^3+1.4454\times10^{-7}(T-273)^3$	atm	[39]
The saturation pressure of methanol vapor	p_{MV}^{sat}	$k_{H,M}x_{M,l}$	atm	[14]
Thermodynamic voltage	V_0	1.21	V	[14]
Transfer coefficient of anode reaction step 1	α_{a1}	0.5	–	[1]
Transfer coefficient of anode reaction step 2	α_{a2}	0.5	–	[1]
Transfer coefficient of cathode	α_c	1.0	–	[18]
Cathode exchange current density	$A_{v,c}j_{0,O_2}^{ref}$	1.14×10^3	A m^{-3}	[18]
Anode reference concentration	C_M^{ref}	1000	mol m^{-3}	[1]
Cathode reference concentration	$C_{O_2}^{ref}$	0.52	mol m^{-3}	[18]

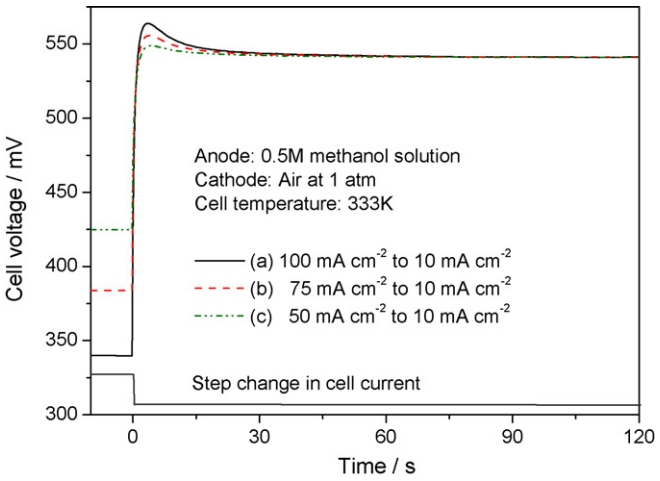

Fig. 2. Dynamic behavior of the cell voltage in response to the current density change from (a) 100 to 10 mA cm^{-2}, (b) 75 to 10 mA cm^{-2}, and (c) 50 to 10 mA cm^{-2}.

40 mA cm^{-2}. Note that in all the cases, the decrement in current density is kept the same as 50 mA cm^{-2}. Interestingly, the voltage overshoot becomes weaker with increasing the initial current density. This result is qualitatively consistent with the experimental findings [23].

In order to clarify the dominant factor that causes the voltage overshoot in response to a change in current density, the time-dependent behaviors of both the anode and cathode overpotentials are plotted in Fig. 4. Clearly, in response to the decrease in current density, the anode overpotential drops suddenly from a higher level to a lower level for all the cases studied, due primarily to the decrease in the charge transfer resistance of the anode electrode reaction. Unlike the anode overpotential, the cathode overpotential shows a significant undershooting, which is believed to be the main reason that results in the cell voltage overshoot. Also, it can be found that it takes about 30 s for the anode overpotential to reach a new steady-state, whereas it takes almost 60 s for the cathode overpotential to reach a new steady-state after the current density changes. The different time characteristics imply the different physicochemical processes occurring in each electrode. In the following, we discuss about the effects of different physicochemical processes on the cell dynamic operation characteristics.

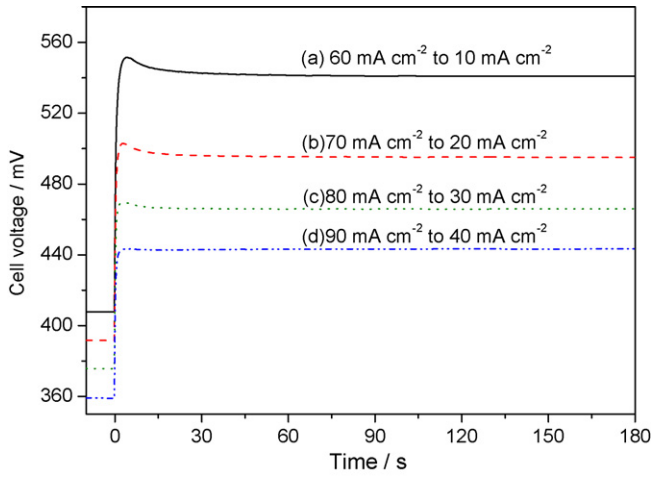

Fig. 3. Dynamic behavior of the cell voltage in response to the current density change of (a) 60 to 10 mA cm^{-2}, (b) 70 to 20 mA cm^{-2}, (c) 80 to 30 mA cm^{-2}, and (d) 90 to 40 mA cm^{-2}.

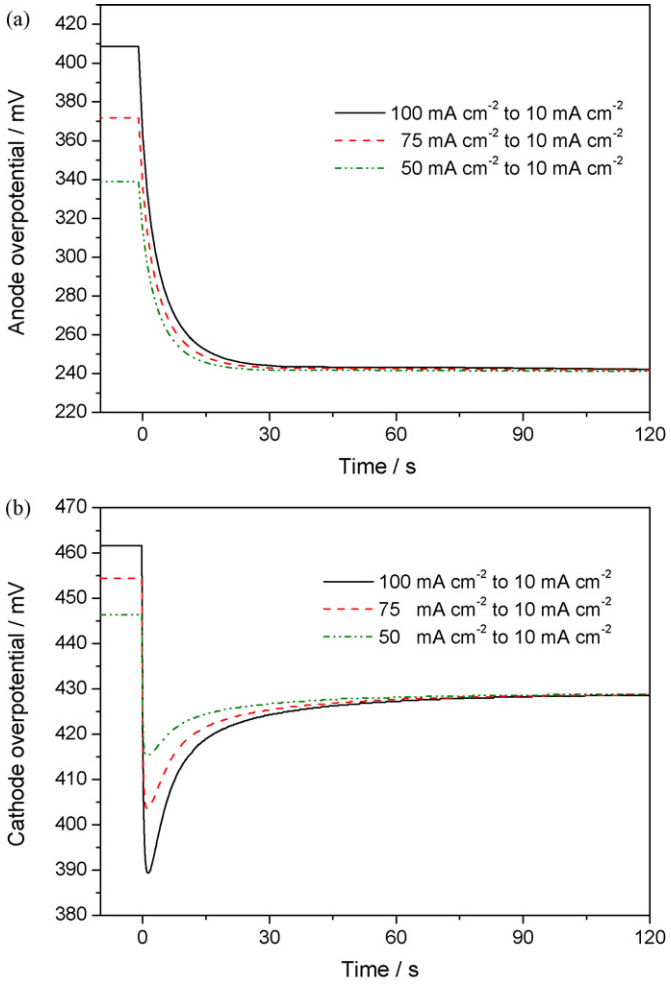

Fig. 4. Dynamic behaviors of (a) anode overpotential and (b) cathode overpotential in response to the change in current density.

3.2. The impact of the double layer capacitance

To make clear the influence of the double layer capacitance, we compare (a) the model that takes account the impact of the DLC and (b) the model that ignores the impact of the DLC. The results are shown in Fig. 5. Clearly, the voltage overshoot becomes weaker with the consideration of DLC. This result suggests that the DLC can smoothen the change in voltage in response to the change in cell current. Also, it is noticed that the impact of the DLC is transitory, which only reacts on the dynamic voltage within a few seconds after the current density changes because the DLC charging/discharging process is generally very fast.

3.3. Surface coverage of CO on the Pt catalyst in the ACL

As indicated in Eq. (25), the adsorbed CO species on the Pt catalyst, θ_{CO}, known as catalyst poisoning, is closely related to the kinetics of MOR and thus may play a role on the anode performance as the current density changes. Fig. 6 shows the time-dependent variation of θ_{CO} in response to the changes in current density. Normally, θ_{CO} is relatively small when the fuel cell discharges at a stably high current density. As the current density suddenly drops, there are more free Pt catalyst sites than needed for the complete methanol oxidation, so methanol adsorption and the dehydrogenation step become prevailing, which consequently results in an increase in θ_{CO}. Clearly, as seen from Fig. 6, the surface coverage

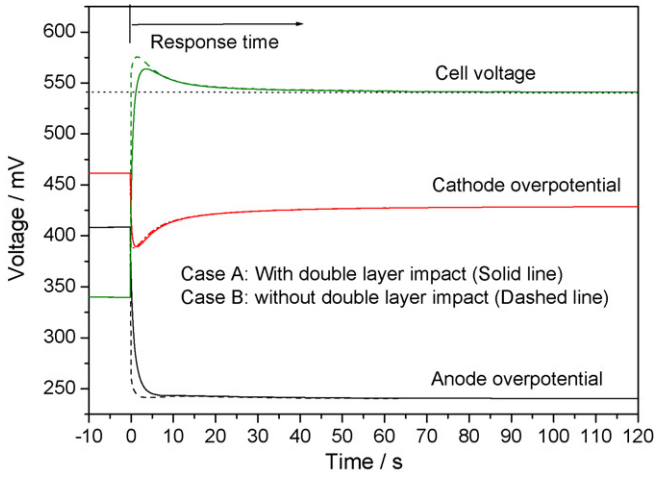

Fig. 5. Dynamic behaviors of the anode overpotential, the cathode overpotential and the cell voltage in response to the change in current density from 100 to 10 mA cm^{-2}. Case A: with the double layer capacitance; Case B: without the double layer capacitance.

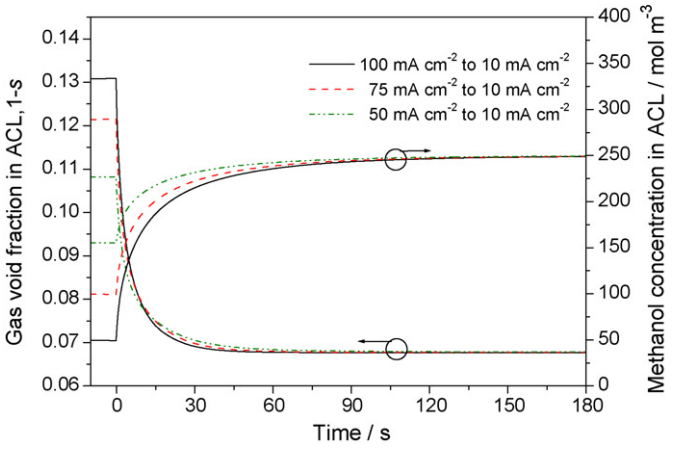

Fig. 7. Dynamic behaviors of the methanol concentration and gas void fraction in the ACL in response to the change in current density.

of CO species on Pt catalyst increases from around 0.44 to around 0.84 when the current density drops from 100 to 10 mA cm^{-2}. With respect to the time characteristic of the catalyst poisoning process, it takes over 60 s for θ_{CO} to reach a new steady-state. However, it is noticed that although there has been large variation in θ_{CO} after the current density changes, the anode overpotential exhibits a relatively constant value for the case without consideration of double layer capacitance, as shown in Fig. 5. This indicates that the anode overpotential is relatively insensitive to the change in surface coverage of CO species on Pt catalyst in the ACL. This result is consistent with the work by Krewer and Sundmacher [23].

3.4. Mass transport of methanol in the DMFC

Another important parameter that may influence the kinetics of the anode electrode reaction is the methanol concentration in the ACL. Fig. 7 shows the time-dependent variations in methanol concentration and gas void fraction in the ACL in response to the changes in current density. As the current density is suddenly decreased, the demand of the methanol for electro-oxidation is decreased, thus breaking the original balance of methanol in the anode electrode. Consequently, the methanol begins to accumulate in the ACL until it reaches a new steady-state, as can be seen in the Fig. 7. Finally, the methanol concentration in the ACL reaches the same steady-state value because the final current densities for all cases studied are the same. Generally, it takes over 90 s for the methanol concentration in the ACL to reach a new steady-state, showing that the mass transport of methanol is sluggish in the liquid feed DMFC. It should be pointed out that although the methanol concentration in the ACL is greatly changed after the current density drops, it does not show a significant influence on the anode overpotential, probably because the kinetics of the anodic MOR is insensitive to methanol concentration once it exceeds a certain value [14,32]. Similar to the methanol transport, the transport of the gas in the ACL is also relatively slow. As shown in the figure, it takes approximate 60 s for the gas void faction in the ACL to reach a new steady-state. To have a deeper understanding of the dynamic characteristics of the methanol transport in the DMFC, the time-dependent variations in methanol concentration in different regions inside the cell are displayed in Fig. 8. The methanol concentrations at six representative regions inside the DMFC are probed, i.e.: the middle points of the ADL, the ACL and the membrane under the midlines of the channel and the rib. As can be seen from Fig. 8, the methanol concentration in each region increases in response to the sudden drop in current density. In particular, the variation in methanol concentration in the ACL is much steeper and larger than in the other regions. Generally, it takes about 45 s for the methanol concentration under the midline of the channel to reach a new steady-state, as shown in Fig. 8a. In contrast, almost 3 min is needed for the methanol concentration under the midline of the rib to reach a new steady-state, as shown in Fig. 8b. The longer response of the methanol concentration in the regions under the rib is resulted from the large transfer resistance and longer transfer distance for the methanol in those regions. The evolution of the methanol concentration profile across the membrane electrode assembly under the centerline of the channel is displayed in Fig. 9. As can be seen from this figure, the methanol concentration in the ACL and its adjacent regions responds very fast within the first second after the current density drops, whereas in other regions far away from the ACL the methanol concentration remains almost the same. This hysteresis is attributed to the slow diffusion of the methanol through the ADL and the MEM.

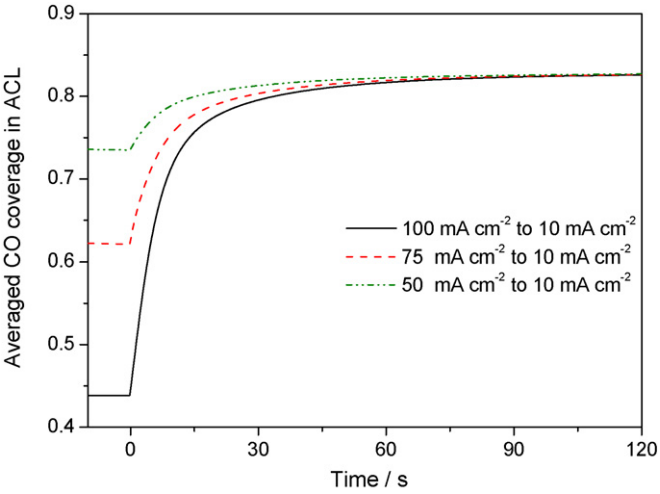

Fig. 6. Dynamic behavior of the CO surface coverage (θ_{CO}) in the ACL in response to the change in current density.

The variations in the methanol concentration in the ACL and in the MEM can significantly influence the flux of methanol permeation through the membrane to the cathode. Fig. 10 shows the

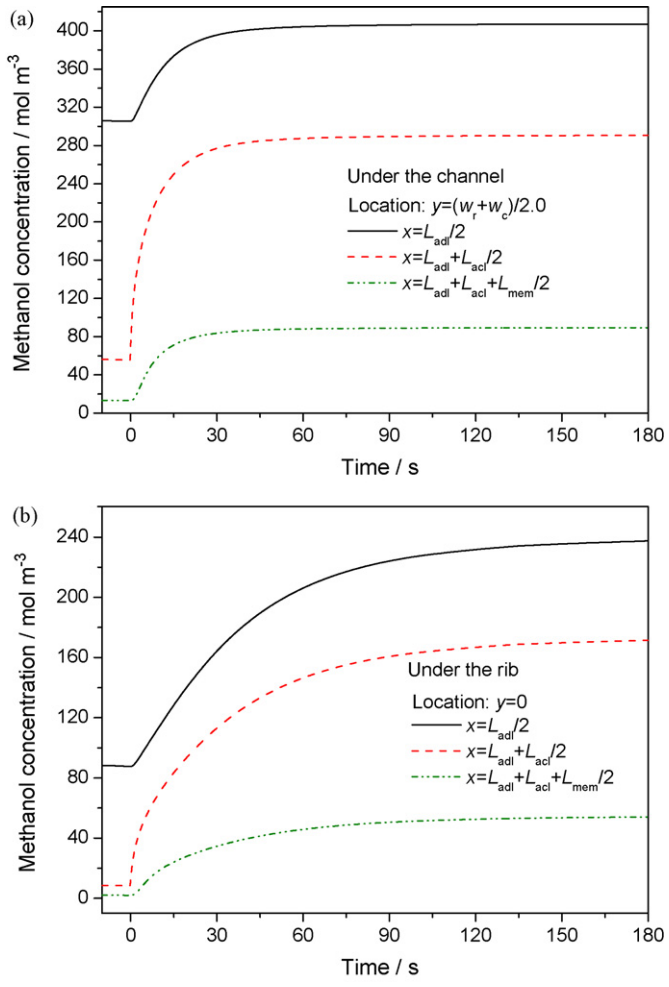

Fig. 8. Dynamic behavior of the methanol concentration in anode electrode and membrane in response to the change in current density from 100 to 10 mA cm^{-2}.

time-dependent behavior of the methanol crossover in response to current density changes. Note that flux of methanol crossover is expressed in terms of the 'parasitic' current density. As can be seen, the flux of methanol crossover gradually increases in response to the drop in current density. It takes over 90 s for the flux of methanol

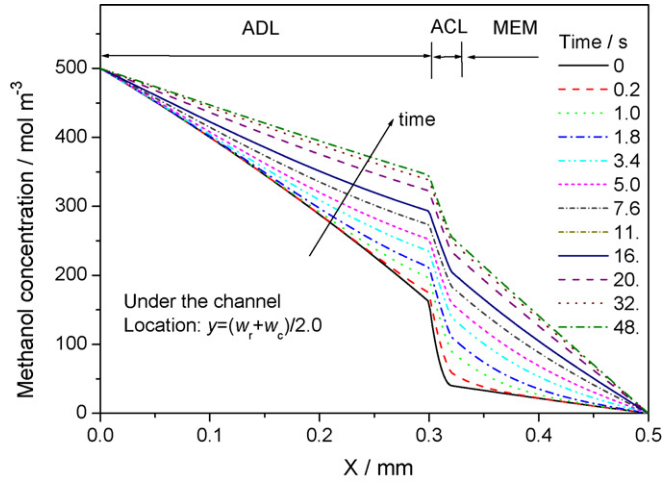

Fig. 9. Dynamic evolution of the methanol concentration profiles through the MEA under the centerline of the channel in response to the change in current density from 100 to 10 mA cm^{-2}.

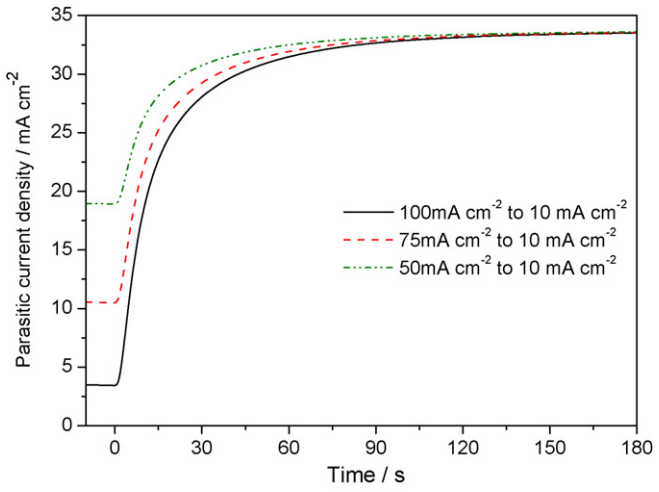

Fig. 10. Dynamic behavior of the methanol crossover in response to the change in current density.

crossover to reach a new steady-state. The time characteristics of the methanol crossover are obviously in the same time range as the methanol concentration increase in the ACL. As concluded earlier, the dynamic methanol crossover results in the dynamic response of cathode mixed overpotential, which has proved to be the dominant reason that results in the cell voltage overshoot behavior.

3.5. Mass transport of oxygen and water in the CCL

Both the oxygen concentration and water saturation in the CCL change with the current density, which in turn may affect the cathode performance. Fig. 11 shows the time-dependent variations in oxygen concentration and liquid saturation in the CCL in response to the changes in current density. As can be seen, the oxygen concentration increases to a relatively higher value within a few seconds resulting from the sudden decrease in the current density. Then, it gradually decreases and reaches a steady-state. The whole process takes over 90 s. With respect to the liquid saturation in the CCL, it gradually decreases to a new steady-state in response to the current density drop. Although both the oxygen concentration and the liquid saturation in the CCL change with a sudden drop in current density, the variation is relatively small for operating conditions considered. However, it should be mentioned that the liquid saturation in the CCL may have a significant impact on the cathode

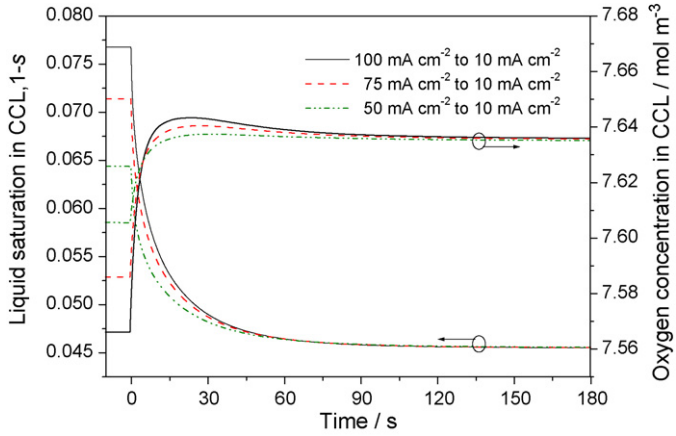

Fig. 11. Dynamic behaviors of the oxygen concentration and liquid water saturation in the CCL in response to the change in current density.

performance wherever the water flooding is becoming serious in the DMFC cathode electrode.

4. Conclusions

A transient, two-dimensional, two-phase mass transport model is developed to investigate the dynamic operating behavior of a liquid feed DMFC. Various processes that may affect the cell operating dynamics are studied. The numerical results show that the transient voltage exhibits a significant overshoot in response to a sudden change in current. The degree of the overshoot depends on the magnitude of the change in current density and the value of the initial current density. It is found that the methanol permeation through the membrane to the cathode results in a strong cathode overpotential overshoot, which is the predominated reason that leads to the voltage overshoot behavior. In contrast, the anode overpotential is found to be insensitive to the change in methanol concentration and CO surface coverage in the ACL. The effect of double layer capacitance on the cell dynamic operation is also studied and the results show that the DLC can smoothen the change in voltage in response to the change in cell current. The dynamic response of mass transport to a change in current density is found to be rather slow. In particular, it is shown that the slow mass transport of methanol is one of the key factors that influence the cell dynamic operation.

Acknowledgements

The work described in this paper was supported by a grant from the Research Grants Council of the Hong Kong Special Administrative Region, China (Project no. 622706) and by the Joint Research Fund for Hong Kong and Macao Young Scholars (Project no. 50629601).

References

[1] K. Sundmacher, T. Schultz, S. Zhou, K. Scott, M. Ginkel, E. Gilles, Chem. Eng. Sci. 56 (2001) 333–341.
[2] S. Zhou, T. Schultz, M. Peglow, K. Sundmacher, Phys. Chem. Chem. Phys. 3 (2001) 347–355.
[3] P. Argyropoulos, K. Scott, W. Taama, J. Power Sources 87 (2000) 153–161.
[4] P. Argyropoulos, K. Scott, W. Taama, Electrochim. Acta 45 (2000) 1983–1998.
[5] J. Kallo, J. Kamara, W. Lehnert, R. von Helmolt, J. Power Sources 127 (2004) 181–186.
[6] C.W. Wong, T.S. Zhao, Q. Ye, J.G. Liu, J. Electrochem. Soc. 152 (2005) A1600–A1605.
[7] P. Argyropoulos, K. Scott, A.K. Shukla, C. Jackson, J. Power sources 123 (2003) 190–199.
[8] A.A. Kulikovsky, J. Electrochem. Soc. 152 (2005) A1121–A1127.
[9] E. Birgersson, J. Nordlund, H. Ekstrom, M. Vynnycky, G. Lindbergh, J. Electrochem. Soc. 150 (2003) A1368–A1376.
[10] J. Nordlund, G. Lindbergh, J. Electrochem. Soc. 149 (2002) A1107–A1113.
[11] A.A. Kulikovsky, J. Divisek, A.A. Kornyshev, J. Electrochem. Soc. 147 (2000) 953–959.
[12] R. Chen, T.S. Zhao, J. Power Sources 152 (2005) 122–130.
[13] G. Murgia, L. Pisani, A.K. Shula, K. Scott, J. Electrochem. Soc. 150 (2003) A1231–A1245.
[14] Z.H. Wang, C.Y. Wang, J. Electrochem. Soc. 150 (2003) A508–A519.
[15] E. Birgersson, J. Nordlund, M. Vynnycky, C. Picard, G. Lindbergh, J. Electrochem. Soc. 151 (2004) A2157–A2172.
[16] J. Divisek, J. Fuhrmann, K. Gartner, R. Jung, J. Electrochem. Soc. 150 (2003) A811–A825.
[17] W.P. Liu, C.Y. Wang, J. Electrochem. Soc. 154 (2007) B352–B361.
[18] W.W. Yang, T.S. Zhao, Electrochim. Acta 52 (2007) 6125–6140.
[19] C. Xu, T.S. Zhao, W.W. Yang, J. Power Sources 178 (2008) 291–308.
[20] R. Chen, T.S. Zhao, W.W. Yang, C. Xu, J. Power Sources 175 (2008) 276–287.
[21] K. Sundmacher, T. Schultz, S. Zhou, K. Scott, M. Ginkel, E.D. Gilles, Chem. Eng. Sci. 56 (2001) 333–341.
[22] T. Schultz, U. Krewer, K. Sundmacher, J. Power Sources 165 (2007) 138–151.
[23] U. Krewer, K. Sundmacher, J. Power Sources 154 (2005) 153–170.
[24] U. Krewer, A. Kamat, K. Sundmacher, J. Electroanal. Chem. 169 (2007) 105–119.
[25] J. Rice, A. Faghri, Int. J. Heat Mass Transfer 49 (2006) 4804–4820.
[26] B. Xiao, A. Faghri, Int. J. Heat Mass Transfer 51 (2008) 3127–3143.
[27] U. Krewer, H.K. Yoon, H.T. Kim, J. Power Sources 175 (2008) 760–772.
[28] D. Natarajan, T.V. Nguyen, J. Electrochem. Soc. 148 (2001) A1324–A1335.
[29] G.Y. Lin, W.S. He, T.V. Nguyen, J. Electrochem. Soc. 151 (2004) A1999–A2006.
[30] W.W. Yang, T.S. Zhao, C. Xu, Electrochim. Acta 53 (2007) 853–862.
[31] W.W. Yang, T.S. Zhao, J. Power Sources 174 (2007) 136–147.
[32] X. Ren, P. Zelenay, S. Thomas, J. Davey, S. Gottesfeld, J. Power Sources 86 (2000) 111–116.
[33] Q. Ye, T.S. Zhao, C. Xu, Electrochim. Acta 51 (2006) 5420–5429.
[34] K. Scott, W.M. Taama, J. Cruichshank, J. Power sources 65 (1997) 159–171.
[35] J.H. Nam, M. Kaviany, Int. J. Heat Mass Transfer 46 (2003) 4595–4611.
[36] S. Um, C.Y. Wang, K.S. Chen, J. Electrochem. Soc. 147 (2000) 4485–4493.
[37] X. Ren, T.E. Springer, T.A. Zawodzinski, S. Gottesfeld, J. Electrochem. Soc. 147 (2000) 466–474.
[38] D. Song, Q. Wang, Z. Liu, T. Navessin, M. Eikerling, S. Holdcroft, J. Power Sources 126 (2004) 104–111.
[39] A. Kazim, H.T. Liu, P. Forges, J. Appl. Electrochem. 29 (1999) 1409–1414.